Electronic Supplementary Material (ESI) for Journal of Materials Chemistry A.

Supplementary information for the manuscript "Increasing the UV and extending into the visible the optical response of TiO_2 through surface activation with highly stable Cu_5 clusters"

María Pilar de Lara-Castells,*,† Andreas W. Hauser,*,‡ José M. Ramallo-López,¶ David Buceta,*,§ Lisandro J. Giovanetti,¶ M. Arturo López-Quintela,§ and Félix G. Requejo¶

†*Instituto de Física Fundamental, C.S.I.C., Serrano 123, E-28006 Madrid, Spain*

‡*Graz University of Technology, Institute of Experimental Physics, Petersgasse 16, 8010 Graz, Austria.*

¶*Instituto de Investigaciones Fisicoquímicas Teóricas y Aplicadas (INIFTA), CONICET and Dto. de Química, Fac. de Ciencias Exactas, UNLP, Argentina*

§*Lab. Nanomag, Instituto de Investigaciones Tecnológicas, Universidad de Santiago de Compostela, E-15782 Santiago de Compostela, Spain*

E-mail: Pilar.deLara.Castells@csic.es; Andreas.W.Hauser@gmail.com; David.Buceta@usc.es

Contents

S1 Experimental diffuse reflectance spectroscopy measurements

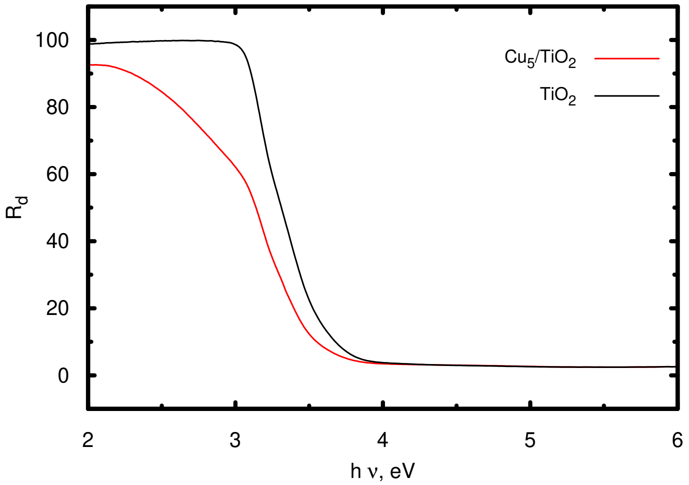

Figure S1: Diffuse Reflectance Spectroscopy (DRS) spectra obtained for the TiO_2 NP (black) and TiO_2 NP modified with Cu_5 clusters (red) as a function of the incipient photon energy $\hbar\nu$.

Figure S1 shows the Diffuse Reflectance Spectroscopy (DRS) spectra for the TiO_2 nanoparticle (NP) and TiO_2 NP modified with Cu_5 clusters as a function of the photon energy ($\hbar\nu$). These spectra show the typical behavior expected for a TiO_2 semiconductor consisting of a nearly flat region, at small photon energies, that is dominated by reflection and scattering due to the high refractive index of the investigated material. The abrupt decrease in R_d, when radiation becomes more intensively absorbed with increasing energy corresponds to an onset of transmission near the optical absorption.

S2 Experimental X-ray fluorescence measurements

As mentioned in the main manuscript, in order to determine the Cu/Ti ratio in the modified sample we perform XRF (X-Ray fluorescence) measurements. S2 shows the obtained XRF spectra using an excitation energy of 10.5 keV to excite the Cu K-edge and the Ti K-edge.

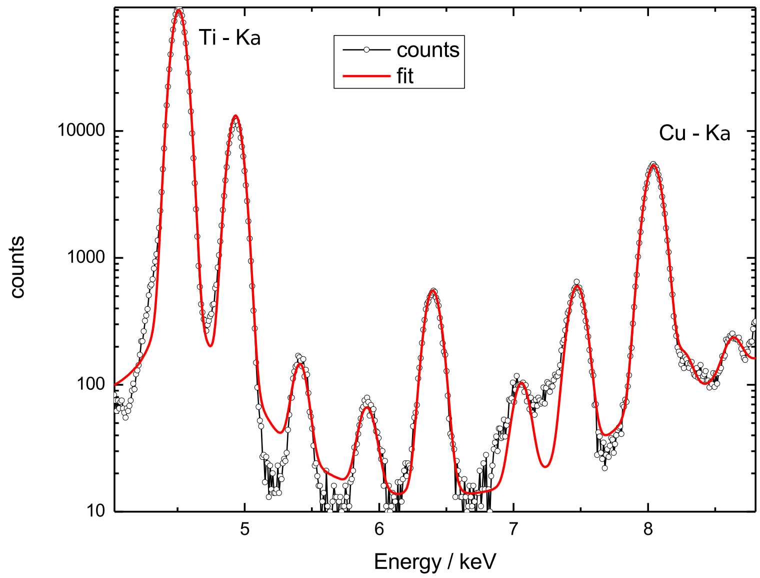

Figure S2: X-Ray Fluorence (XRF) spectra obtained for the TiO_2 NP modified with Cu_5 clusters. All peaks different from those of Ti and Cu were identified as stemming from the sample holder and sample environment and are at least one order of magnitude less intense than those under analysis (Ti and Cu).

As mentioned in the main text, using PyMca X-ray Fluorescence Toolkit,[1] of the emission lines intensity of Ti and Cu (Ti-Kα and Cu-Kα), and taking into account every correction factor (cross section, thickness, filters, etc), it was possible to determine that the Cu/Ti atomic ratio in the modified TiO_2 NP sample was 0.018(4).

S3 Experimental XANES spectra at the Ti K edge

We have also carried out XANES spectra at the Ti K-edge trying to identify possible changes in the electronic structure of Ti atoms. Figure S3 presents the XANES spectra for the TiO_2 NP and TiO_2 NP modified with Cu_5 clusters. It can be seem that both spectra are almost indistinguishable, showing no appreciable changes at the Ti atoms. Note that the XANES spectra obtained by transmission mode are the result of the average of all Ti atoms in the sample, which indicates that there is only a small fraction Ti atoms on the TiO_2 nanoparticle surface which is directly interacting with the Cu_5 clusters.

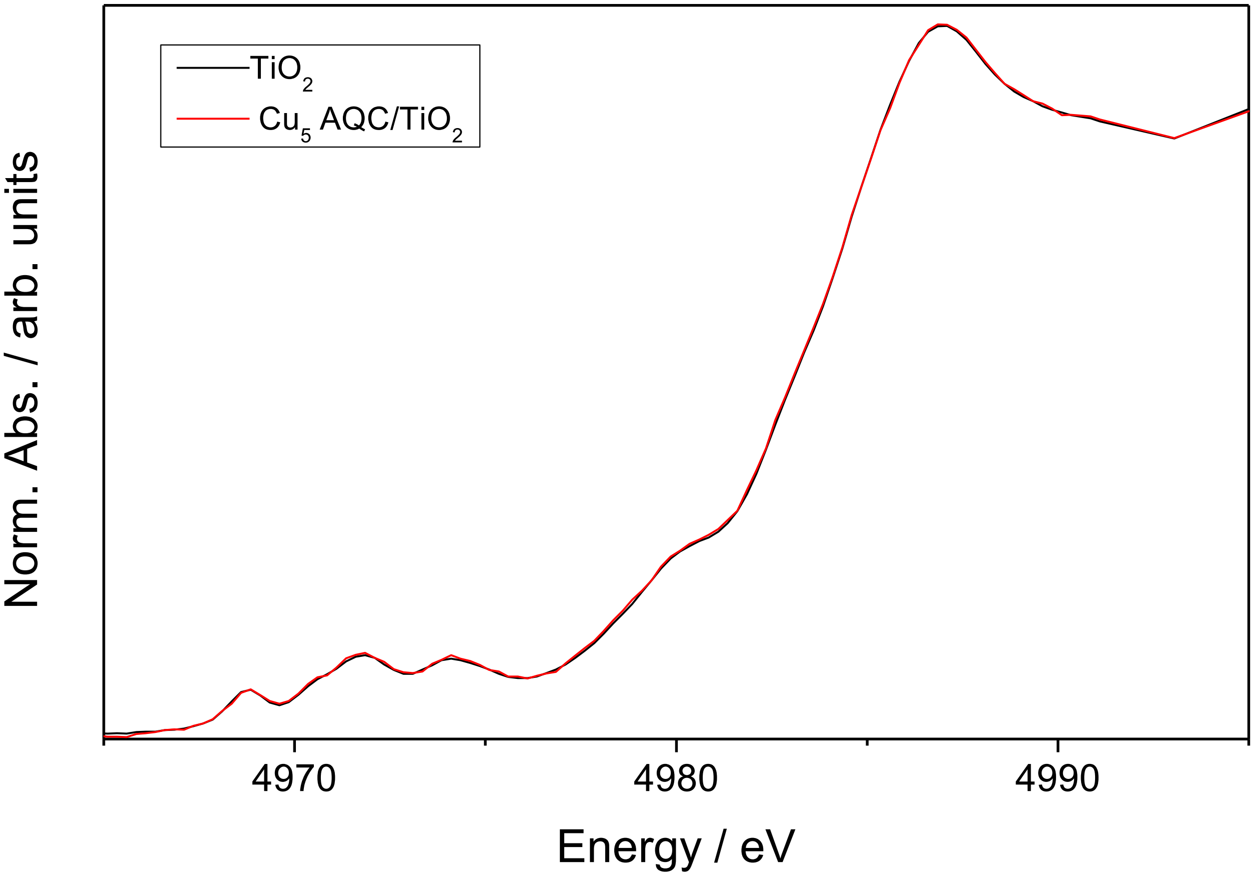

Figure S3: XANES spectra at the Ti K-edge of TiO_2 NP (black line) and TiO_2 NP modified with Cu_5 clusters (red line).

S4 Transmission electron microscopy (TEM) of TiO_2 nanoparticles

Transmission Electron Microscopy (TEM) images were obtained with a JEOL JEM- 2010 microscope, working at an accelerating voltage of 100kV. A drop from a diluted sample solution was deposited onto an amorphous carbon film on 400 mesh copper grids and left to evaporate at room temperature.

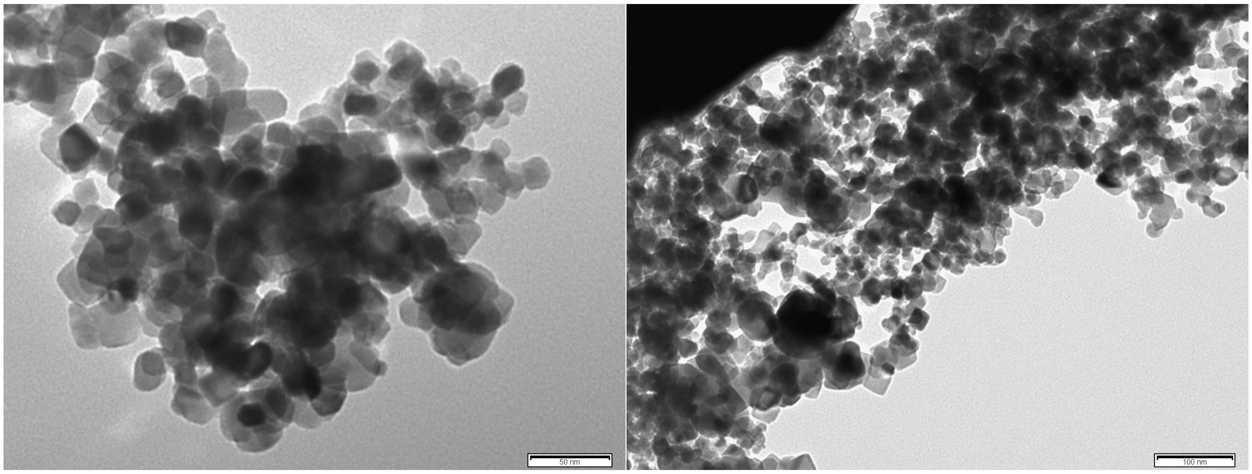

Figure S4: TEM micrographs of the TiO_2 nanoparticles used for the experiments showing the presence of aggregates.

S5 Radial scans of Cu_5(trapezoidal-shaped)/TiO_2(110) interaction energies

Radial scans of Cu_5/TiO_2(110) interaction energies as a function of the distance between Cu_5 and the surface are presented in S5. As discussed in the main manuscript (sections 2.1 and 4.3), the radial scans were obtained using the PBE-D3 approach. The trapezoidal (gas-phase)) structure of the Cu_5 cluster, as adsorbed onto two positions of the TiO_2(110) surface, are shown in S6. Notice that the information on the potential minima from S6 is presented in Figure 2 of the main manuscript.

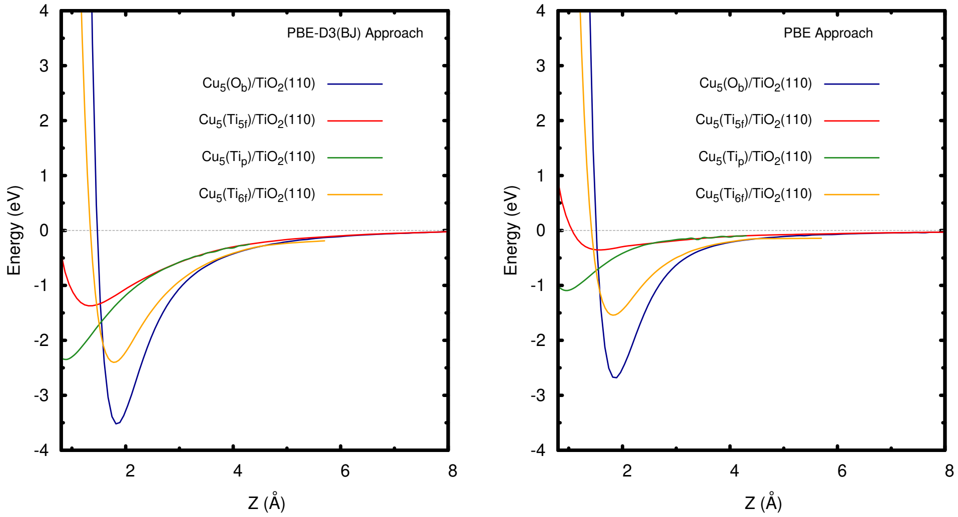

Figure S5: Comparison of $Cu_5/TiO_2(110)$ interaction energies using the PBE-D3(BJ) scheme (left-hand panel) and the vdW-uncorrected PBE approach (right-hand panel). The central Cu atoms are located: (1) on top of the five-fold coordinated Ti_{5f} atom (Ti_{5f} site, as shown in S6); (2) the bridging oxygen atom O_b (O_b site, as shown in S6); (3) hollow site atop the titanium atoms on the 2^{nd}-molecular-layer (Ti_{sub} site); (4) atop sixfold coordinated titanium atoms (Ti_{6f} site). Z (in Å) stands for the distance between the central Cu atom and the surface plane where the oxygen bridging atoms are located.

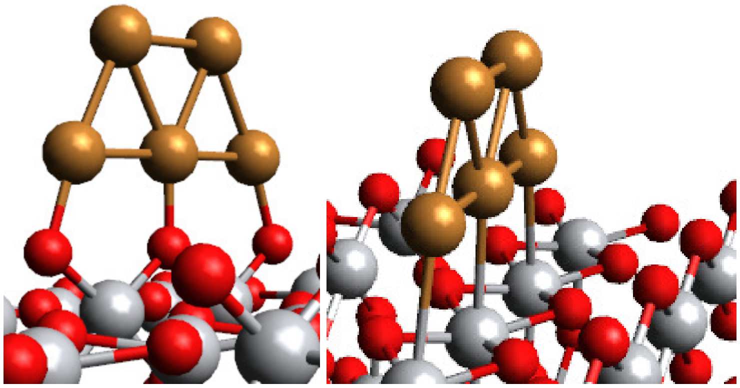

Figure S6: Figure illustrating the $Cu_5/TiO_2(110)$ system with the central Cu atom located on top of the five-fold coordinated Ti_{5f} atom (right-hand panel) and the bridging oxygen atom O_b (left-hand panel).

S6 Complementary results for the Cu_5 (trapezoidal-shaped)/TiO_2 system without including surface relaxation

This section presents complementary results for the Cu_5 (trapezoidal-shaped)/TiO_2 system when the ions of the surface are not relaxed using the HSE06 method.

S6.1 Characterization of the frontier orbitals

This subsection presents tables characterizing the frontier highest-energy double-occupied (HOMO), second double-occupied (HOMO-1) single-occupied (SOMO), and lowest-energy unoccupied (LUMO) molecular orbitals. In particular, the tables are listing the energies of these orbitals, the amount of s, p and d-type character, and the electron localization (Cu_5, Ti or O), obtained by a projection of the one-electron-wavefunctions onto spherical harmonics centered at the ions of the Cu_5 (trapezoidal-shaped)/TiO_2 system.

Table S1: Characterization of frontier orbitals: HOMO, SOMO, and LUMO. Spin-unpolarized calculations.

Energy (eV)	orbital **HOMO**			orbital **SOMO**			orbital **LUMO**		
	-3.1915			-2.4665			-2.4045		
	s	p	d	s	p	d	s	p	d
Cu_5	0.418	0.143	0.346	0.0	0.0	0.0	0.0	0.0	0.0
O	0.007	0.034	0.040	0.0	0.026	0.0	0.0	0.034	0.0
Ti	0.0	0.007	0.046	0.026	0.0	0.949	0.026	0.0	0.940

S6.2 Characterization of the most relevant orbitals in the photoexitation

This subsection compares the composition of the orbitals involved in the most intense absorption peaks in the infrared, visible, and UV regions of the photoabsorption spectra of

Table S2: Characterization of frontier occupied (HOMO and SOMO) and unoccupied (LUMO) molecular orbitals. Spin-polarized calculations. Majority spin component.

	orbital **HOMO**			orbital **SOMO**			orbital **LUMO**		
	Majority spin component								
Energy (eV)	-3.2641			-2.7888			-2.4316		
	s	p	d	s	p	d	s	p	d
Cu_5	0.417	0.143	0.348	0.0	0.0	0.0	0.0	0.0	0.0
O	0.007	0.034	0.040	0.0	0.034	0.0	0.0	0.034	0.0
Ti	0.0	0.007	0.045	0.028	0.0	0.939	0.025	0.0	0.941

Table S3: Characterization of frontier occupied (HOMO) and unoccupied (referred to us LUMO and LUMO+1) molecular orbitals. Spin-polarized calculations. Minority spin component.

	orbital **HOMO**			orbital **LUMO**			orbital **LUMO+1**		
	Minority spin component								
Energy (eV)	-3.2644			-2.4317			-2.3561		
	s	p	d	s	p	d	s	p	d
Cu_5	0.417	0.143	0.348	0.0	0.0	0.0	0.0	0.0	0.0
O	0.007	0.034	0.0	0.0	0.034	0.0	0.0	0.009	0.0
Ti	0.0	0.007	0.045	0.025	0.0	0.941	0.0	0.009	0.983

Cu_5-decorated TiO_2. Color coding refers to Figure S7, which shows the absorption spectra with peak contributions highlighted by arrows of the same color. The majority spin components are presented.

Table S4: Characterization of the orbitals involved in the electronic excitation providing the dashed orange transition in Figure S7.

	orbital 540			orbital 611		
	s	p	d	s	p	d
Cu_5	0.0	0.0	0.0	0.001	0.0	0.003
O	0.0	0.034	0.0	0.0	0.101	0.0
Ti	0.028	0.0	0.939	0.001	0.010	0.884

Table S5: Characterization of the orbitals involved in the electronic excitation providing the green transition in Figure S7.

	orbital 538			orbital 596		
	s	p	d	s	p	d
Cu_5	0.017	0.015	0.900	0.002	0.004	0.009
O	0.002	0.041	0.0	0.0	0.036	0.0
Ti	0.0	0.004	0.020	0.004	0.002	0.949

Table S6: Characterization of the orbitals involved in the electronic excitation providing the black transition in Figure S7.

	orbital 536			orbital 576		
	s	p	d	s	p	d
Cu_5	0.006	0.001	0.969	0.003	0.001	0.0
O	0.0	0.016	0.0	0.001	0.055	0.0
Ti	0.0	0.0	0.008	0.004	0.013	0.922

Table S7: Characterization of the orbitals involved in the electronic excitation providing the red transition in Figure S7.

	orbital 533			orbital 583		
	s	p	d	s	p	d
Cu_5	0.011	0.002	0.957	0.0	0.0	0.0
O	0.00	0.019	0.0	0.00	0.069	0.0
Ti	0.0	0.0	0.011	0.007	0.021	0.902

Table S8: Characterization of the orbitals involved in the electronic excitation providing the blue transition in Figure S7.

	orbital 499			orbital 549		
	s	p	d	s	p	d
Cu_5	0.0	0.0	0.001	0.0	0.0	0.0
O	0.0	0.902	0.00	0.0	0.028	0.0
Ti	0.005	0.028	0.064	0.002	0.004	0.965

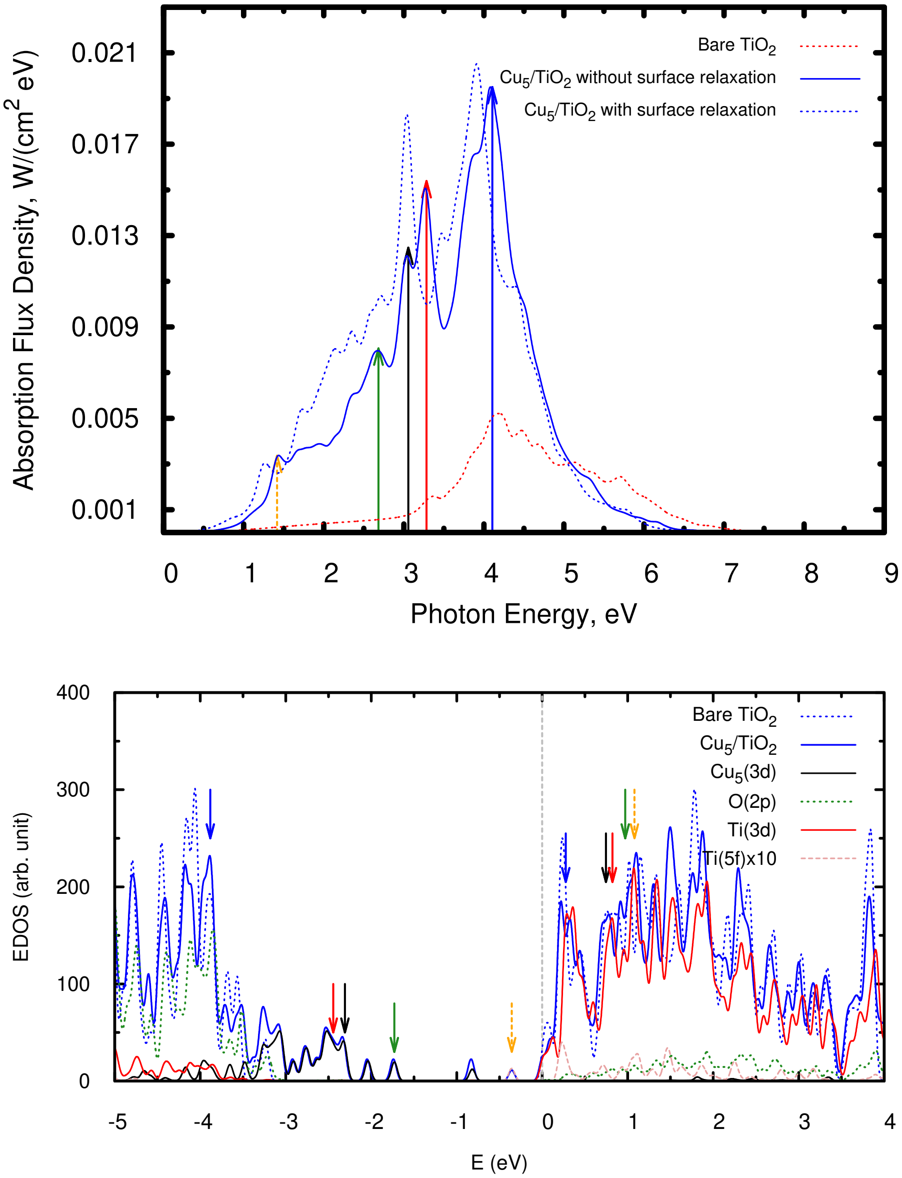

Figure S7: Upper panel: Photo-absorption spectra of the $TiO_2(110)$ surface, without adsorbates (red lines) and with the adsorbed Cu_5 cluster (blue lines). The positions of the most intense peaks is also indicated. Bottom panel: Electronic density of states (EDOS) of the bare $TiO_2(110)$ surface and the Cu_5-$TiO_2(110)$ system. The zero of energy is set to the energy of the lowest unoccupied molecular orbital (LUMO). The projected density of states onto O(2p), Ti(3d), and Cu(3d) orbitals is also shown as well as that projected on the 3d orbitals from the nearest Ti(5f) ion. The arrows indicate the bands responsible for the most intense peaks in the spectrum (upper panel).

S7 Complementary results for the Cu_5 (trapezoidal-shaped)/TiO_2 system including surface relaxation

This section presents complementary results for the Cu_5 (trapezoidal-shaped)/TiO_2 system when the ions of the surface are relaxed, as shown in section 2.3 of the main manuscript.

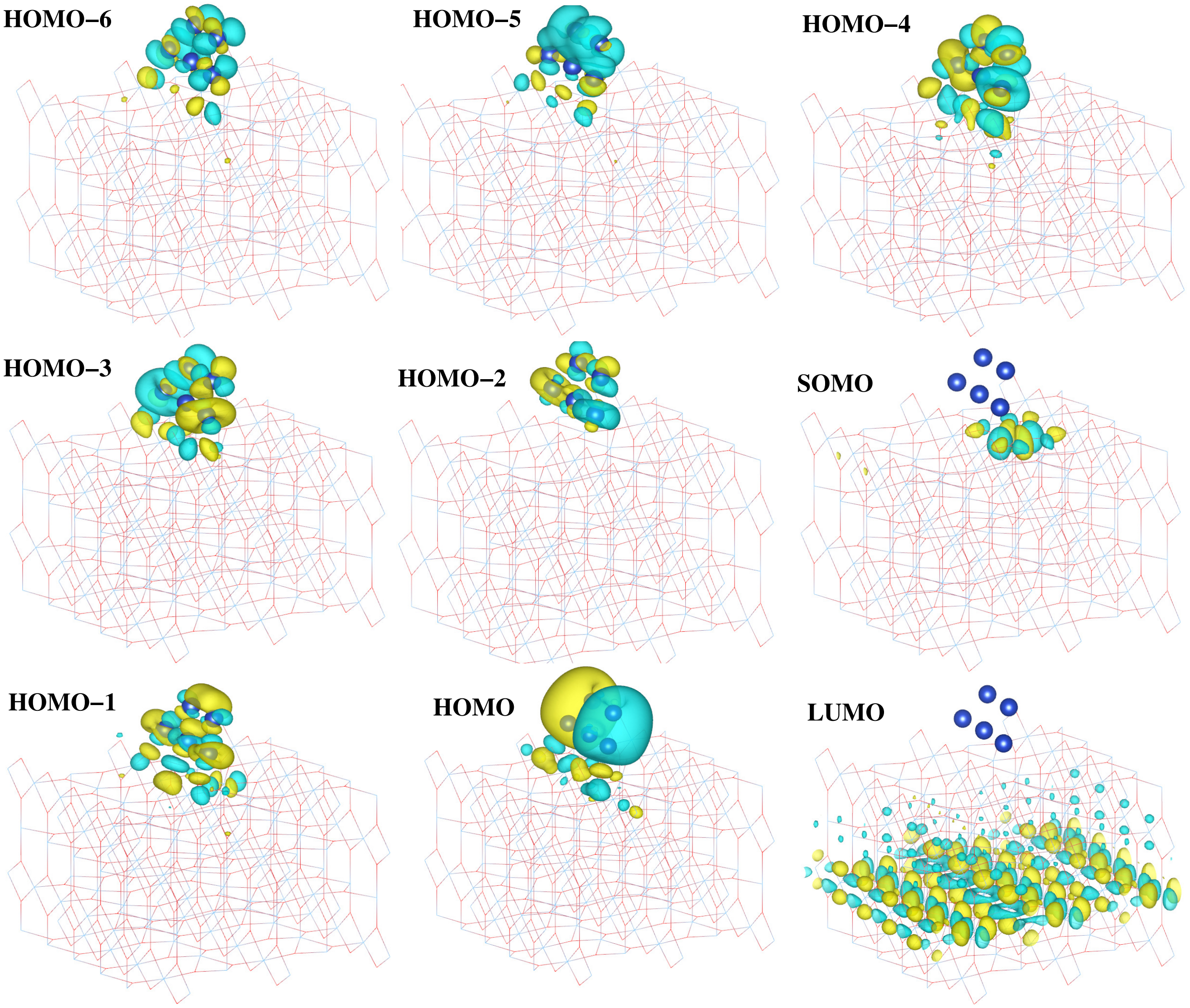

Figure S8: Picture illustrating iso-density surfaces of frontier orbitals for (trapezoidal-shaped) Cu_5 adsorbed on the $TiO_2(110)$ Surface. Spin-polarized calculations including relaxation.

S7.1 Characterization of the frontier orbitals

This subsection presents tables characterizing the frontier highest-energy double-occupied (HOMO), single-occupied (SOMO), and lowest-energy unoccupied (LUMO) molecular orbitals. In particular, the tables are listing the energies of these orbitals, the amount of s, p and d-type character, and the electron localization (Cu_5, Ti or O), obtained by a projection of the one-electron-wavefunctions onto spherical harmonics centered at the ions of the Cu_5 (trapezoidal-shaped)/TiO_2 system.

Table S9: Characterization of frontier occupied (HOMO-1, HOMO and SOMO) molecular orbitals. Majority spin component.

	orbital **SOMO**			orbital **HOMO-1**			orbital **HOMO**		
	Majority spin component								
Energy (eV)	−3.9528			−3.8623			−3.0070		
	s	p	d	s	p	d	s	p	d
Cu_5	0.0	0.0	0.039	0.014	0.013	0.857	0.420	0.133	0.339
O	0.0	0.063	0.0	0.002	0.043	0.0	0.007	0.029	0.0
Ti	0.015	0.013	0.871	0.002	0.004	0.064	0.0	0.003	0.069

Table S10: Characterization of frontier occupied (HOMO-1,HOMO) and unoccupied (LUMO) molecular orbitals. Minority spin component.

	orbital **HOMO-1**			orbital **HOMO**			orbital **LUMO**		
	Minority spin component								
Energy (eV)	−3.8669			−3.0083			−2.7874		
	s	p	d	s	p	d	s	p	d
Cu_5	0.016	0.015	0.894	0.418	0.132	0.339	0.0	0.0	0.0
O	0.007	0.034	0.0	0.007	0.028	0.0	0.0	0.021	0.0
Ti	0.0	0.007	0.045	0.0	0.007	0.069	0.009	0.004	0.966

S7.2 Characterization of the most relevant orbitals in the photoexitation

This subsection compares the composition of the orbitals involved in the most intense absorption peaks in the infrared, visible, and UV regions of the photoabsorption spectra of Cu_5-decorated TiO_2. Color coding refers to Figure 5 of the main manuscript, which shows the absorption spectra with peak contributions highlighted by arrows of the same color. The majority spin components are presented.

Table S11: Characterization of the orbitals involved in the electronic excitation providing the orange transition in Figure 5 of the main manuscript.

	orbital 540			orbital 609		
	s	p	d	s	p	d
Cu_5	0.420	0.133	0.339	0.007	0.001	0.003
O	0.007	0.029	0.0	0.0	0.082	0.0
Ti	0.0	0.003	0.072	0.013	0.001	0.883

Table S12: Characterization of the orbitals involved in the electronic excitation providing the pink transition in Figure 5 of the main manuscript.

	orbital 540			orbital 609		
	s	p	d	s	p	d
Cu_5	0.0	0.0	0.039	0.0	0.0	0.0
O	0.0	0.063	0.0	0.0	0.031	0.0
Ti	0.015	0.013	0.871	0.0	0.015	0.954

Table S13: Characterization of the orbitals involved in the electronic excitation providing the green transition in Figure 5 of the main manuscript.

	orbital 539			orbital 699		
	s	p	d	s	p	d
Cu_5	0.014	0.013	0.857	0.007	0.001	0.003
O	0.002	0.043	0.0	0.0	0.082	0.0
Ti	0.002	0.004	0.064	0.013	0.011	0.883

Table S14: Characterization of the orbitals involved in the electronic excitation providing the blue transition in Figure 5 of the main manuscript.

	orbital 509			orbital 566		
	s	p	d	s	p	d
Cu_5	0.0	0.0	0.004	0.0	0.0	0.0
O	0.0	0.961	0.0	0.0	0.053	0.0
Ti	0.0	0.004	0.031	0.002	0.010	0.935

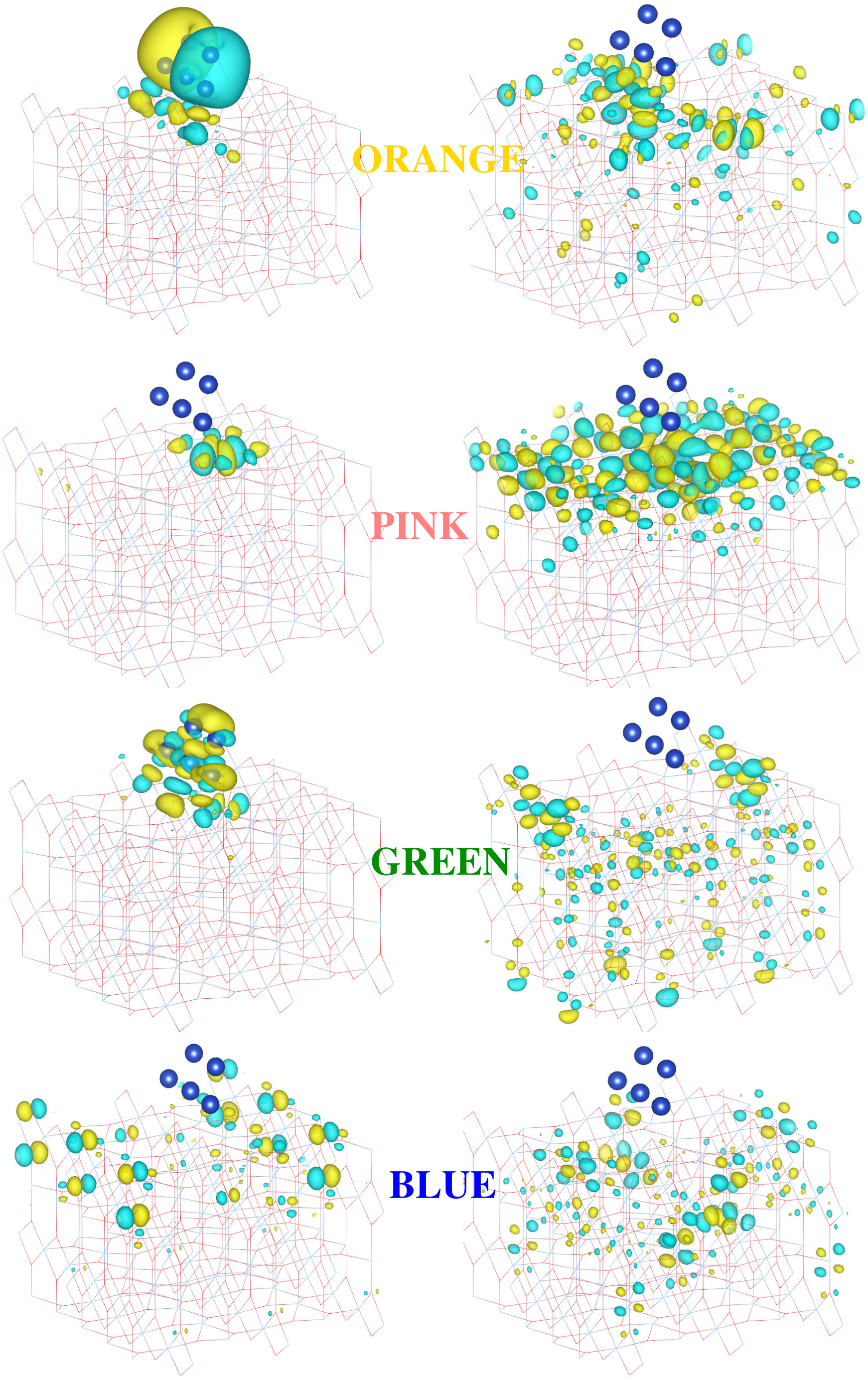

Figure S9: Picture illustrating iso-density surfaces of the orbitals responsible of the absorption spectra with peak contributions highlighted by the same color as the arrows in Figure 5 of the main manuscript.

S8 Complementary results for a rectangular-shaped Cu_5 isomer on the TiO_2 surface

Additional calculations were performed for the rectangular-shaped Cu_5 configuration shown in S10. Upon adsorption and relaxation, the copper cluster adopts a slightly pyramidal structure, with the central atom about 0.58 Å above the base of the pyramidal structure. The distance from the central atom to the Ti(5f) lying right below the cluster was 3.04 Å. The first subsection presents the results obtained without relaxing the surface while the ions of the surface were obtained in getting those shown in the second subsection.

S8.1 Rectangular-shaped Cu_5 isomer on the TiO_2 surface without surface relaxation

In a first set of calculations, the ions of the surface were not relaxed. The most important frontier orbitals are characterized in S15, as calculated with the HSE06 method.

Table S15: Characterization of frontier occupied (HOMO and SOMO) and unoccupied (LUMO) molecular orbitals. Majority spin component.

	orbital **HOMO**			orbital **SOMO**			orbital **LUMO**		
	Majority spin component								
	s	p	d	s	p	d	s	p	d
Cu_5	0.489	0.108	0.177	0.001	0.0	0.0	0.0	0.0	0.0
O	0.0	0.120	0.0	0.0	0.034	0.0	0.0	0.034	0.0
Ti	0.003	0.015	0.086	0.025	0.0	0.939	0.025	0.0	0.941

As can be seen in S11, the profile of the spectra is very similar for the trapezoidal- and rectangular-shaped configurations in the ultraviolet region. The main difference lies in the red-shifting of the most intense peak located in the visible region (by more than 0.5 eV). Since the energy difference between both isomers is just 0.31 eV, it can be expected that both (and other) isomers could co-exist at room temperature, and that the experimental spectrum results from the convolution from different isomers, yielding the continuous profile

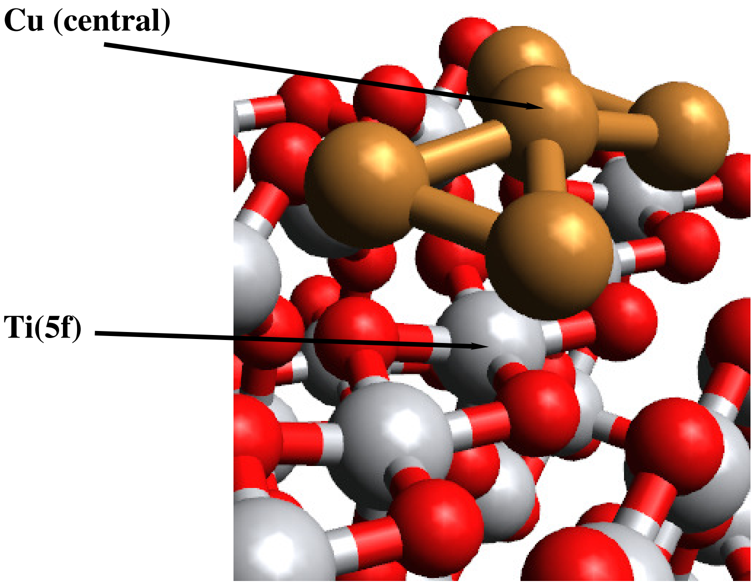

Figure S10: Picture illustrating a rectangular-shaped (local minimum configuration) of the Cu_5 cluster onto the $TiO_2(110)$ surface, with an energy 0.31 eV above that for the lowest-energy (planar trapezoidal) arrangement shown in Figure 1 of the main manuscript (-3.40 vs -3.71 eV).

shown in Figure 4 of the main manuscript.

Table S16: Characterization of the orbitals involved in the electronic excitation providing the pink transition in Figure S8.

	orbital 539			orbital 573		
	s	p	d	s	p	d
Cu_5	0.001	0.0	0.0	0.0	0.0	0.0
O	0.034	0.0	0.0	0.0	0.024	0.0
Ti	0.025	0.0	0.939	0.0	0.002	0.974

The spectra is formed by three main peaks. The absorbance peak located in the infrared region is due to the transfer of the unpaired electron (originally located in the copper cluster) from surface to subsurface Ti atoms (3d $\rightarrow$ 3d transition). The most intense peak of the visible region comes from the direct electron transfer from the highest energy double-occupied HOMO orbital (making of the hybridization of 4s and 3d Cu orbitals with 2p O and 3d orbitals) to Ti(3d) orbitals. Finally, the most intense peak in the UV region involves the transfer of an electron from (mainly) subsurface oxygen atoms to Ti atoms, which are thus

Table S17: Characterization of the orbitals involved in the electronic excitation providing the green transition in Figure S8.

	orbital 539			orbital 573		
	s	p	d	s	p	d
Cu_5	0.489	0.108	0.177	0.056	0.030	0.049
O	0.0	0.12	0.0	0.002	0.073	0.0
Ti	0.003	0.015	0.086	0.016	0.051	0.722

Table S18: Characterization of the orbitals involved in the electronic excitation providing the blue transition in Figure S8.

	orbital 479			orbital 572		
	s	p	d	s	p	d
Cu_5	0.0	0.0	0.004	0.0	0.0	0.0
O	0.0	0.974	0.0	0.0	0.086	0.0
Ti	0.0	0.006	0.017	0.009	0.011	0.894

more prone to accept the electron charge upon the Cu_5 cluster adsorption.

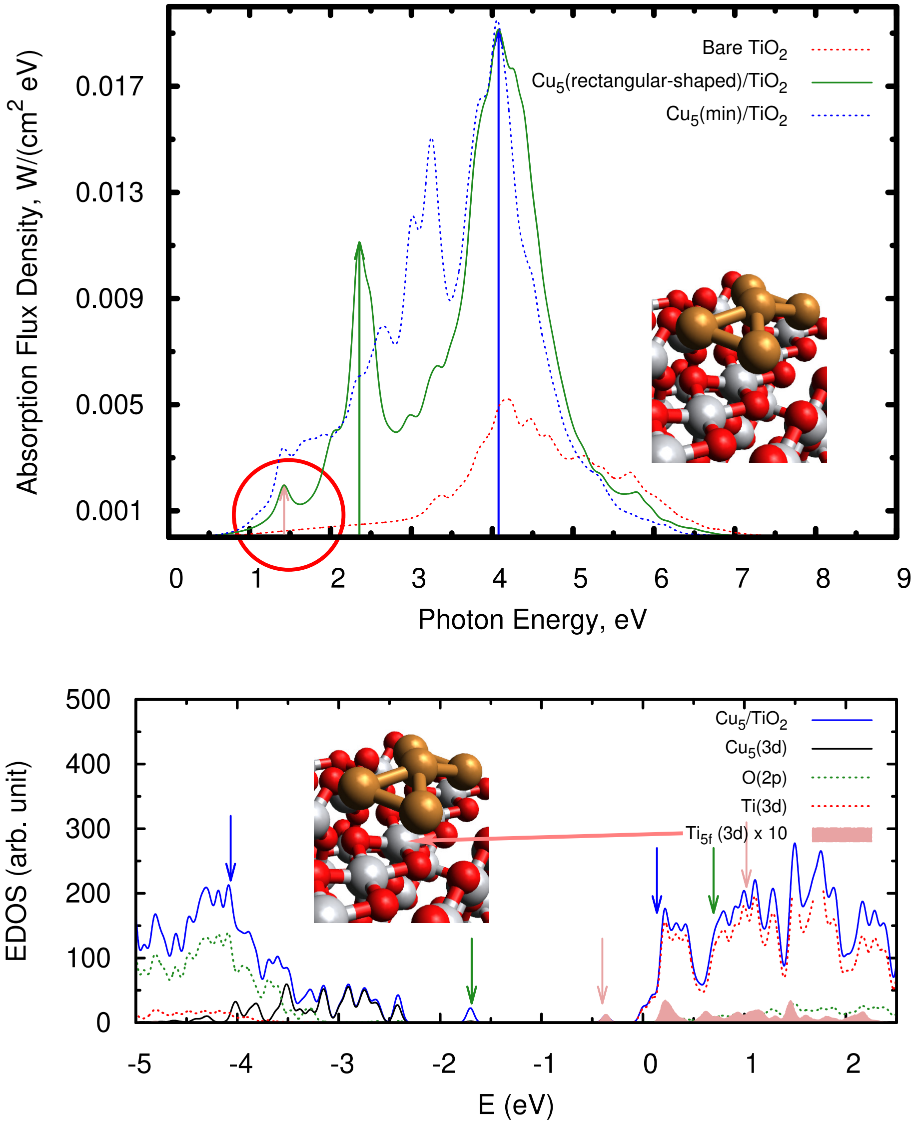

Figure S11: Upper panel: Photo-absorption spectra of the TiO$_2$(110) surface, without adsorbates (dotted red lines), with an adsorbed trapezoidal-shaped (dotted blue lines) and rectangular-shaped Cu$_5$ (forest-green line) configuration, without including surface relaxation. The arrows indicate the position of the most intense peaks. The red circle indicates the transition from the SOMO orbital. Bottom panel: Electronic density of states (EDOS) of the bare TO$_2$(110) surface and the Cu$_5$(trapezoidal-shaped)-TiO$_2$(110) system. The zero of energy corresponds to the energy of the lowest unoccupied molecular orbital (LUMO). The projected density of states onto O(2p), Ti(3d), and Cu(3d) orbitals is also shown. The major composition of the SOMO (pink) orbital is also indicated, as arising from the 3d orbitals located on the Ti$_{5f}$ atom right below the Cu$_5$ cluster (see inset). The arrows indicate the bands responsible for the most intense peaks in the spectrum (upper panel).

S8.2 Rectangular-shaped Cu_5 isomer on the TiO_2 surface including surface relaxation

Additional calculations were performed including surface relaxation, using the procedure briefly described in the main manuscript: First, the PBE-D3 method was applied as described, but with the Hubbard term (DFT+U) added. The values of U reported in a previous study of Cu_n clusters ($n \leq 4$) onto the (101) and (100) surfaces of anatase[2] were used (4.2 eV for titanium and 5.2 eV for copper). All atomic positions were relaxed in the PBE+U/D3 calculations. This procedure resulted in the identification of a small polaron Ti^{3+} $3d^1$ state. Using the PBE+U method, the value of the band-gap for the bare TiO_2 surface was 2.4 eV, which underestimates the experimental value by more than 0.5 eV. In contrast, the HSE06 method provided a good value for the band-gap of titania instead (about 3.2 eV) and was applied starting with the polaronic solution found from the application of the DFT+U/D3 approach.

The resulting electronic density of states is presented in S12, as calculated for the planar rentangle-like isomer shown in the inset of the figure. The frontier orbitals are characterized by the values presented in S19. As indicated in the EDOS(see S12), a midgap state (marked in pink color) has been identified as a polaronlike state formed in a Ti(6f) atom adjacent to the Ti(5f) atom lying right below the center of the copper cluster. It has been tested that the change in the magnetic moment for this localized Ti^{3+} $3d^1$ state was about 0.9 μ_B. In contrast, the copper cluster completely lost its magnetic moment upon adsorption on titania. As shown in S19, the SOMO orbital, occupied by the unpaired electron (originally located on the copper cluster), is dominated by the 3d orbitals of the Ti atoms (by about 90%). Specifically, it is mostly composed of the $3d_{z^2}$ orbital of the Ti^{3+} state (by about 70%). A Bader analysis reveals that the copper cluster donates about 1.09 $|e|$ of its charge, mostly received by the Ti^{3+} ion.

It can be observed that the photo-absorption spectra and EDOS shown in S12 shares very similar characteristics to that calculated without the polaron formation. The most noticeable difference is in fact in the localization of the EDOS from the SOMO midgap state in just one Ti atom. A higher intensity and shifting to the visible region of the spectrum is found for the peak associated with the photo-induced transfer of the electron initially located in the SOMO orbital (i.e., the "Ti^{3+}" surface ion) to 3d orbitals in the conduction band arising from subsurface Ti atoms.

Table S19: Characterization of frontier occupied (HOMO and SOMO) and unoccupied (LUMO) molecular orbitals. Majority spin component.

	orbital **HOMO**			orbital **SOMO**			orbital **LUMO**		
	Majority spin component								
	s	p	d	s	p	d	s	p	d
Cu_5	0.377	0.153	0.139	0.004	0.001	0.0	0.0	0.0	0.0
O	0.003	0.118	0.0	0.0	0.082	0.0	0.0	0.017	0.0
Ti	0.006	0.030	0.173	0.002	0.015	0.895	0.009	0.0	0.974

Table S20: Characterization of frontier occupied (HOMO) and unoccupied (referred to us LUMO and LUMO+1) molecular orbitals. Spin-polarized calculations. Minority spin component.

	orbital **HOMO**			orbital **LUMO**			orbital **LUMO+1**		
	Minority spin component								
	s	p	d	s	p	d	s	p	d
Cu_5	0.388	0.157	0.141	0.0	0.0	0.0	0.0	0.0	0.0
O	0.003	0.118	0.0	0.0	0.034	0.0	0.0	0.017	0.0
Ti	0.006	0.032	0.155	0.009	0.0	0.957	0.0	0.0	0.983

Finally, it can be clearly observed in S13 that the agreement with the experiment is clearly better when considering the lowest-energy (trapezoidal-shaped) structure and not the rectangular-shaped isomer. This is also indicating that the Cu_5 cluster might conserve its gas-phase trapezoidal-shaped structure upon adsorption.

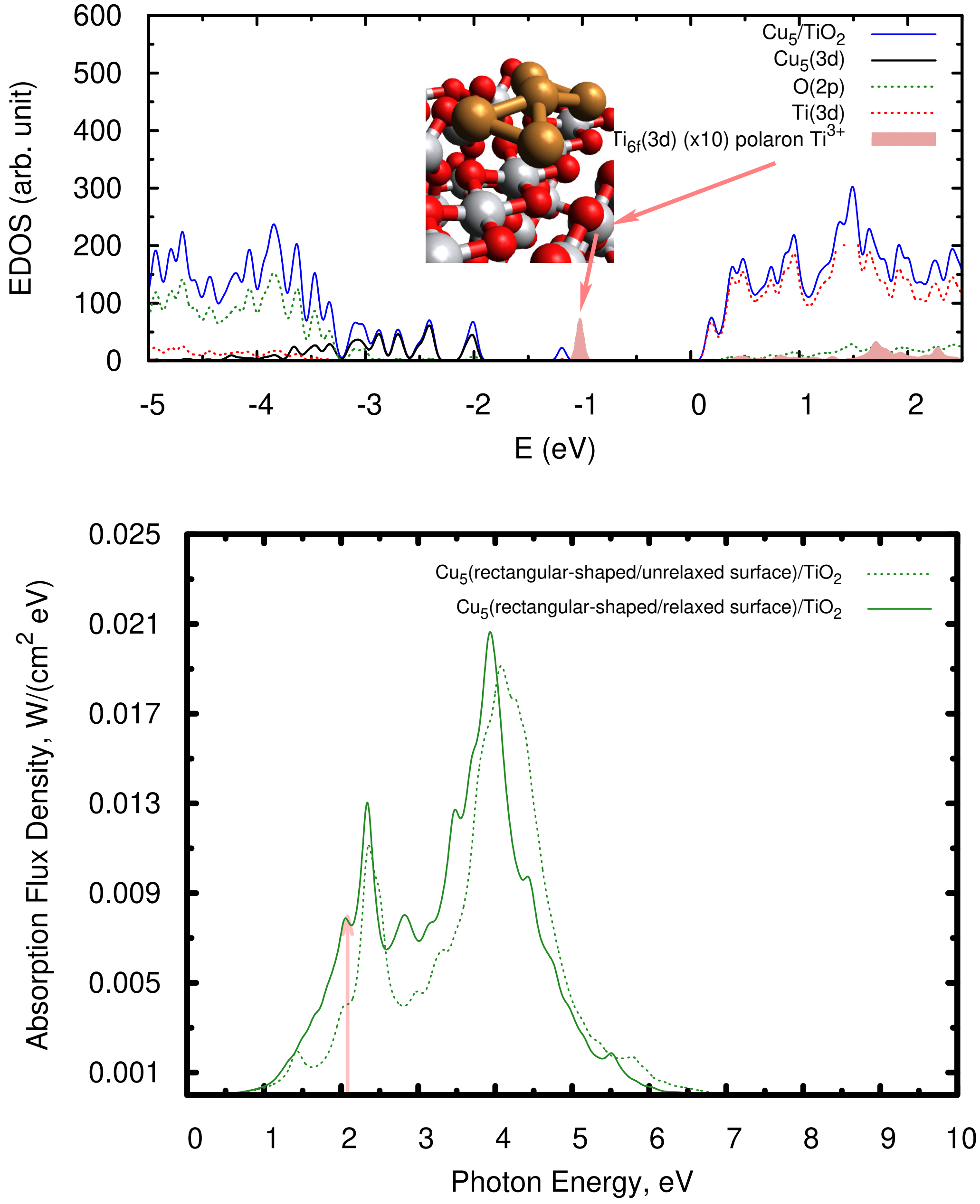

Figure S12: Upper panel: Electronic density of states (EDOS) of the bare $TiO_2(110)$ surface and the Cu_5-$TiO_2(110)$ system, shown together with the projected density of states onto O(2p), Ti(3d), and Cu(3d) orbitals. The pink arrows indicate the position of a polaronic Ti^{3+} ion (located at Ti(6f)) in the vicinity of the Cu_5 cluster. Bottom panel: comparison of the photo-absorption spectra without a polaronic state (dashed green) and with a polaronic state (green). The major contribution of the SOMO orbital (from the Ti^{3+} atom) is also indicated with a pink arrow.

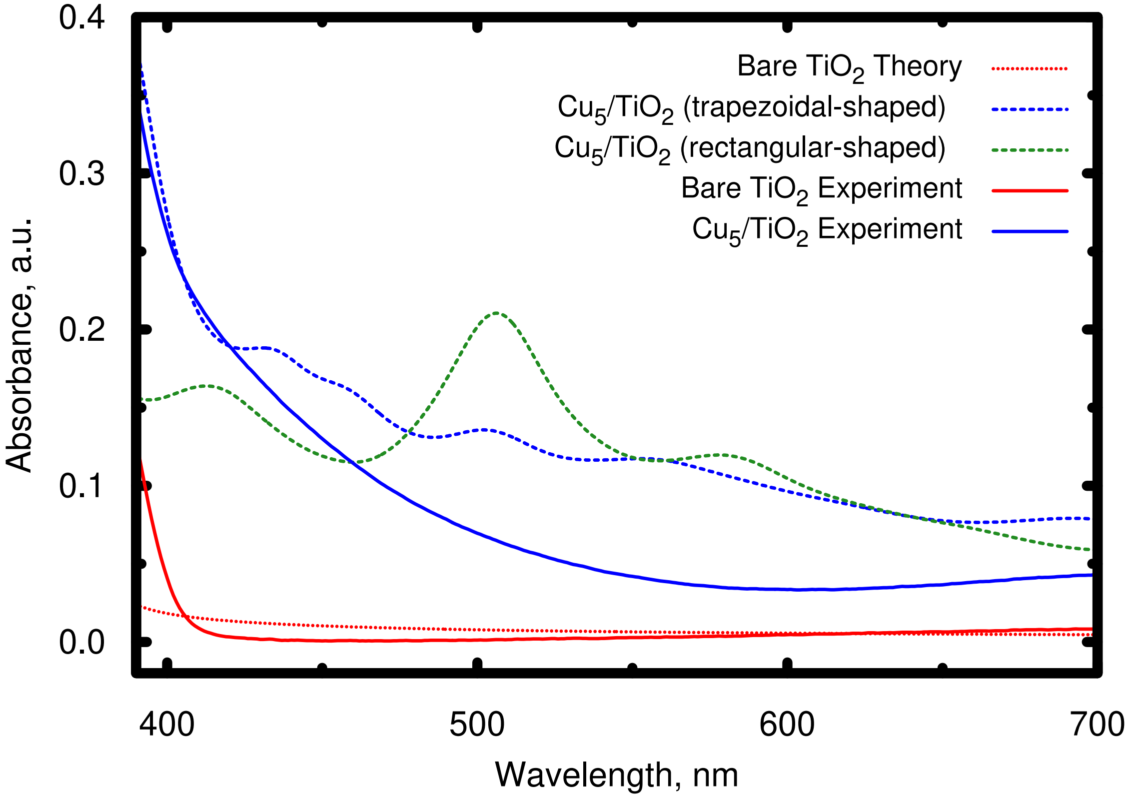

Figure S13: Comparison of the theoretical and experimental absorbance in the visible region. The experimental absorbance A has been calculated via diffuse reflectance spectroscopy (DRS) measurements from the diffuse reflectance signal R_d as $A = log_{10}(1/\mathrm{R}_d)$ (see section S1 of the Supplementary Information for the details of the diffuse reflectance spectra measurements.)

S9 Cluster model calculations

As a complement of the periodic DFT-based study, cluster model calculations were performed by applying the PBE-D3(BJ) scheme with the `ORCA`[3] suite of programs (version 4.0.1.2). For this purpose, an atom-centered def2-SPV[4] basis set was used for copper atoms while the (augmented) polarized correlation-consistent triple-ζ (aug-cc-pVTZ) basis of Woon and Dunning, Jr.,[5] as reported in Ref. 6, was employed for oxygen and titanium atoms. As can be observed in S14 (bottom panel), the highest occupied (HOMO) and second highest occupied (HOMO-1) molecular orbitals share very similar profiles to those calculated via periodic calculations (see S8). As expected from the lack of the DFT+U Hubbard term in PBE calculations, the charge density from the (single-occupied) SOMO orbital becomes delocalized in surface and subsurface Ti ions instead of being localized on a single Ti atom (the cation labelled as Ti(5f) in S8).

Notice from the Löwdin reduced orbital charges presented in S21 that the cluster model predicts a net charge transfer from Cu_5 to TiO_2 with the Cu($3d$) orbitals being the atomic orbitals losing more population upon adsorption. This might explain the enhancement of the Cu($3d^9$) signature in the XANES spectra of the Cu_5/TiO_2 system. A charge transfer from d to s-type orbitals of Cu atoms can be also identified so that the population of the s-type orbitals centered on the Cu atoms labelled as Cu(4) and Cu(5) in S8 is increased upon adsorption. This way, the highest (mostly s-like) HOMO orbital, which is single-occupied in the free Cu_5 cluster, turns out to be double-occupied in the Cu_5/TiO_2 system, with the associated spin density becoming insignificant (see Löwdin reduced spin analysis in S22).

An anti-ferromagnetic arrangement of the electrons on Cu($3d^9$) atomic configurations might be also invoked to explain why the reduced spin density are negligible on these orbitals (see S22). This is clearly reflected in the largest atomic projections of the HOMO-1 orbital: the Cu($3d_{z^2}$) atomic orbitals centered on the Cu(1) and Cu(2) atoms (see S8). Notice also that the anti-ferromagnetic configuration is favored by the superexchange interaction with the bridging oxygen anion (labelled as O_b in the upper panel of S8) connecting the Cu(1) and Cu(2) atoms in the Cu_5/TiO_2 system.

The comparison of the frontier orbitals of the free Cu_5 clusters and the Cu_5/TiO_2 system provides further insights into the binding mechanism (see bottom panel of S8):

- The HOMO-1 orbital, composed by $3d$ atomic contributions from four Cu atoms in the free cluster, becomes dominated by $3d_{z^2}$ contributions centered on the Cu(1) and Cu(2) atoms, presenting a clear mixing with the $2\mathrm{p}_z$ orbitals of the bridging oxygen atoms lying right below these Cu atoms, and thus signaling a partial covalent nature of the Cu_5/TiO_2 binding. The energy of the HOMO-1 orbital in the free Cu_5 cluster (-4.49 eV) is very close to that of the HOMO orbital in the TiO_2 system and represented in S15 (-4.20 eV), easing the mixing of Cu($3d$) and O($2p$) contributions.
- The HOMO orbital, double-occupied and composed by $3d$ atomic contributions from all Cu atoms in the free cluster, can be correlated with the single-occupied SOMO orbital in the Cu_5/TiO_2 system, dominated by Ti($3d$) atomic contributions, and thus signaling the donation of one electron from the Cu_5 cluster to the TiO_2 surface.
- The SOMO orbital, single-occupied and composed by $4s$ atomic contributions from all Cu atoms in the free cluster, becomes double-occupied and dominated by $4s$ contributions centered on the Cu(4) and Cu(5) atoms, and thus reflecting an internal charge transfer within the Cu_5 cluster itself: from the atoms labelled as Cu(1), Cu(2), and Cu(3) in S8 to the atoms labelled as Cu(4) and Cu(5) in the same picture.

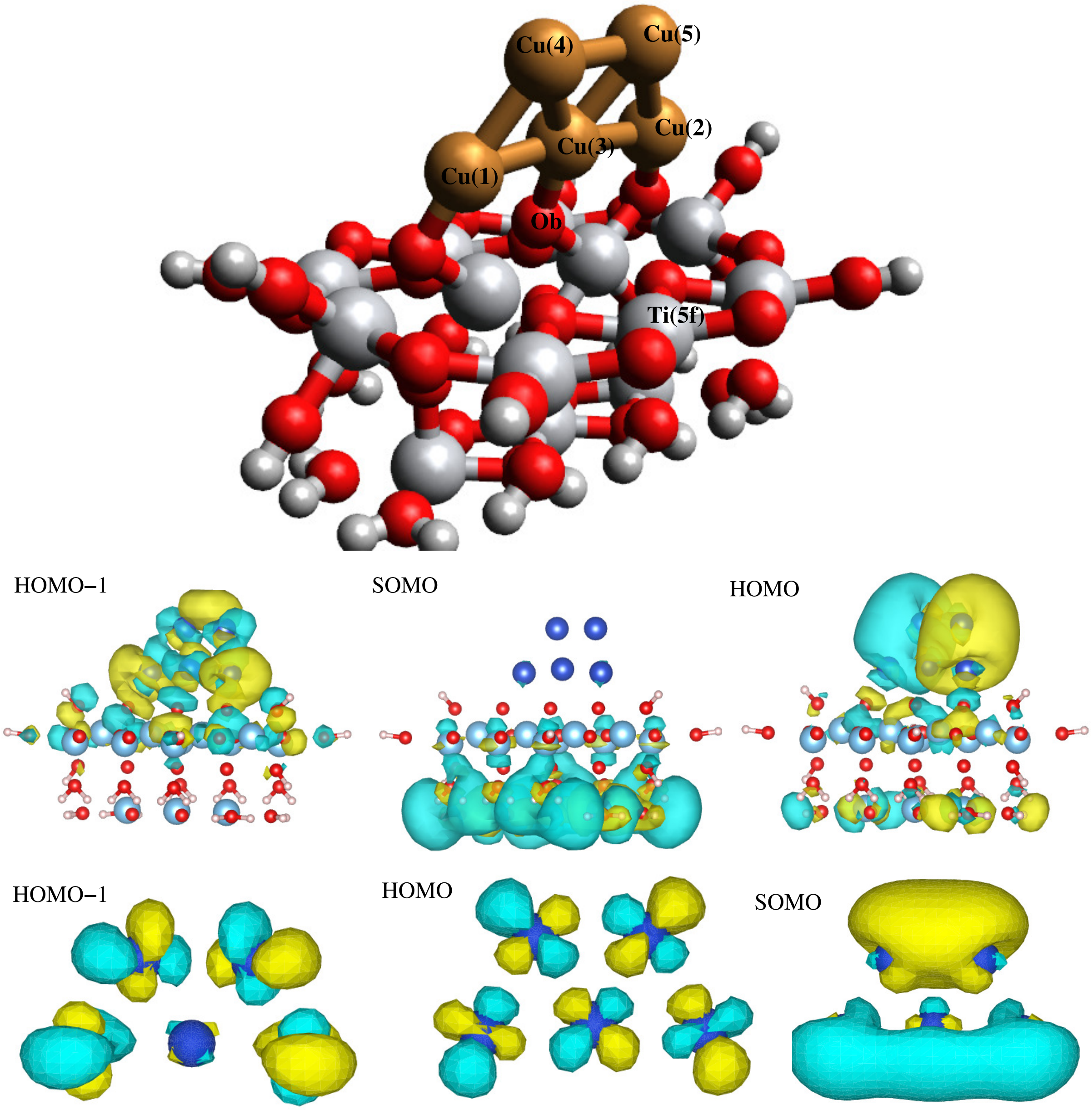

Figure S14: Upper panel: Figure illustrating the hydrogen-saturated cluster used to model the $Cu_5-TiO_2(110)$ interaction. Middle panel: iso-density surfaces of HOMO-1, SOMO, and HOMO orbitals in the Cu_5/TiO_2 system. Bottom panel: iso-density surfaces of HOMO-1, HOMO, and SOMO orbitals in the free Cu_5 cluster. The iso-density surfaces from the majority spin component are represented.

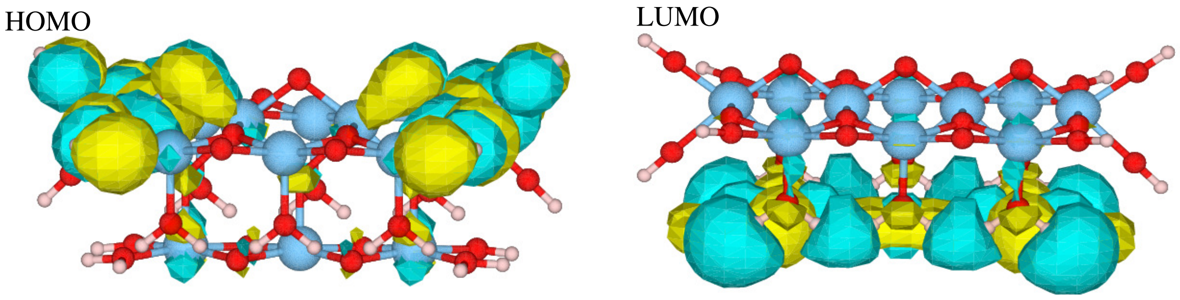

Figure S15: Iso-density surfaces of HOMO and LUMO orbitals in the free TiO_2 cluster.

Table S21: Löwdin reduced orbital charges. The Cu atoms are enumerated as in S14 (upper panel). A minus (plus) sign in the values listed in the last column indicates the loss (gain) of charge upon adsorption on TiO_2.

	Free Cu_5	**Cu_5/TiO_2**	**Difference**
Cu(1) *s*	6.739644	6.695643	−0.044001
Cu(1) *p*	12.58991	12.58481	0.0
Cu(1) *d*	9.721650	9.563318	−**0.158332**
Cu(1) total			−0.202333
Cu(2) *s*	6.739644	6.695643	−0.044001
Cu(2) *p*	12.58991	12.58481	0.0
Cu(2) *d*	9.721650	9.563318	−**0.158332**
Cu(2) total			−0.202333
Cu(3) *s*	7.011063	6.791302	−0.219656
Cu(3) *p*	12.15735	12.38492	+0.227582
Cu(3) *d*	9.809488	9.636041	−**0.173336**
Cu(3) total			−0.165410
Cu(4) *s*	6.853209	7.104205	+0.250996
Cu(4) *p*	12.36348	12.22220	−0.141280
Cu(4) *d*	9.779748	9.706388	−**0.073360**
Cu(4) total			+0.036356
Cu(5) *s*	6.853209	7.104205	+0.250996
Cu(5) *p*	12.36348	12.22220	−0.141280
Cu(5) *d*	9.779748	9.706388	−**0.073360**
Cu(5) total			+0.036356
Total			
Cu_5 *s*	34.19677	34.39100	+**0.194334**
Cu_5 *p*	62.06413	61.99894	−**0.054978**
Cu_5 *d*	48.81228	48.17545	−**0.636720**
Cu_5 total	145.0	144.5	−**0.497364**

Table S22: Löwdin reduced spin populations. The Cu atoms are enumerated as in S14 (upper panel). A minus (plus) sign in the values listed in the last column indicates the loss (gain) of spin population upon adsorption onto $\mathbf{TiO_2}$.

	Free $\mathbf{Cu_5}$	**$\mathbf{Cu_5/TiO_2}$**	**Difference**
Cu(1) *s*	0.063979	0.000748	−0.063231
Cu(1) *p*	0.075212	−0.003821	−0.079033
Cu(1) *d*	0.043589	−0.006849	−0.050438
Cu(1) total			**−0.192702**
Cu(2) *s*	0.063979	0.000748	−0.063231
Cu(2) *p*	0.075212	−0.003821	−0.079033
Cu(2) *d*	0.043589	−0.006849	−0.050438
Cu(2) total			**−0.192702**
Cu(3) *s*	0.131216	−0.005143	−0.136359
Cu(3) *p*	0.021749	−0.004340	−0.026089
Cu(3) *d*	0.020922	−0.004430	−0.025252
Cu(3) total			**−0.187700**
Cu(4) *s*	0.142083	−0.014032	−0.156115
Cu(4) *p*	0.074963	−0.005401	−0.080364
Cu(4) *d*	0.017665	−0.013616	−0.031281
Cu(4) total			**−0.267760**
Cu(5) *s*	0.142083	−0.014032	−0.156115
Cu(5) *p*	0.074963	−0.005401	−0.080364
Cu(5) *d*	0.017665	−0.013616	−0.031281
Cu(5) total			**−0.267760**
		Total	
Cu_5 *s*	0.543340	−0.034703	**−0.575051**
Cu_5 *p*	0.322099	−0.022784	**−0.344883**
Cu_5 *d*	0.143430	−0.045360	**−0.188690**
Cu_5 total	1.0	−0.1	**−1.108624**

References

(1) Solé, V.; Papillon, E.; Cotte, M.; Walter, P.; Susini, J. A Multiplatform Code for the Analysis of Energy-Dispersive X-ray Fluorescence Spectra. *Spectrochim. Acta, Part B* **2007**, *62*, 63 – 68.

(2) Seriani, N.; Pinilla, C.; Crespo, Y. Presence of Gap States at Cu/TiO_2 Anatase Surfaces: Consequences for the Photocatalytic Activity. *J. Phys. Chem. C* **2015**, *119*, 6696–6702.

(3) Neese, F. Software update: the ORCA program system, version 4.0. *Wiley Interdiscip. Rev.: Comput. Mol. Sci.* **2018**, *8*, e1327.

(4) Weigend, F.; Ahlrichs, R. Balanced Basis Sets of Split Valence, Triple Zeta Valence and Quadruple Zeta Valence Quality for H to Rn: Design and Assessment of Accuracy. *Phys. Chem. Chem. Phys.* **2005**, *7*, 3297–3305.

(5) Woon, D. E.; Dunning, Jr., T. H. Gaussian Basis Sets for Use in Correlated Molecular Calculations. Calculation of Static Electrical Response Properties. *J. Chem. Phys.* **1994**, *100*, 2975–2988.

(6) de Lara-Castells, M. P.; Stoll, H.; Mitrushchenkov, A. O. Assessing the Performance of Dispersionless and Dispersion-Accounting Methods: Helium Interaction with Cluster Models of the TiO_2(110) Surface. *J. Phys. Chem. A* **2014**, *118*, 6367–6384.